Inverse Kinematic and Dynamic Analyses of 6-DOF PUS Type Parallel Manipulators

Jong-Phil Kim
Graduate School, Department of Mechatronics, Kwangju Institute of Science and Technology, Kwangju 500-712, Korea
Jeha Ryu*
Department of Mechatronics, Kwangju Institute of Science and Technology, Kwangju 500-712, Korea

This paper presents inverse kinematic and dynamic analyses of HexaSlide type six degree-of-freedom parallel manipulators. The HexaSlide type parallel manipulators(HSM) can be characterized as an architecture with constant link lengths that are attached to moving sliders on the ground and to a mobile platform. In the inverse kinematic analyses, the slider and link motion (position, velocity, and acceleration) is computed given the desired mobile platform motion. Based on the inverse kinematic analysis, in order to compute the required actuator forces given the desired platform motion, inverse dynamic equations of motion of a parallel manipulator is derived by the Newton-Euler approach. In this derivation, the joint friction as well as all link inertia are included. Relative importance of the link inertia and joint frictions on the computed torque is investigated by computer simulations. It is expected that the inverse kinematic and dynamic equations can be used in the computed torque control and model-based adaptive control strategies.

Key Words : Parallel Manipulator, Inverse Kinematics, Inverse Dynamics, Newton-Euler Approach

Nomenclature

$\mathbf{A}_i$: Position vector of i-th universal joint
$\mathbf{B}_i$: Position vector of i-th spherical joint
$\mathbf{I}$: Moment of inertia of mobile platform
$\mathbf{I}_{li}$: Moment of inertia of i-th link
$\mathbf{R}$: Orientation matrix of mobile platform
$\mathbf{R}_{li}$: Orientation matrix of i-th link
$\mathbf{a}_i$: Unit vector along the i-th linear guide
f_{si} : Frictional force at i-th prismatic joint
$\mathbf{f}_{ui}$: Frictional moment at i-th universal joint
$\mathbf{f}_{pi}$: Frictional moment at i-th spherical joint
l : Link length
m_{si} : Equivalent mass of i-th slider part
m_{li} : Mass of i-th link
m : Mass of mobile platform
$\mathbf{n}_i$: Unit vector along i-th link length direction
$\boldsymbol{\omega}$: Angular velocity of mobile platform
$\boldsymbol{\omega}_{li}$: Angular velocity of i-th link
τ_i : Articular force of i-th actuator
$\mathbf{a}^{\times}$: Skew-symmetric matrix

* Corresponding Author,
E-mail : ryu@kjist.ac.kr
TEL : +82-62-970-2389; **FAX** : +82-62-970-2384
Department of Mechatronics, Kwangju Institute of Science and Technology, Kwangju 500-712, Korea.
(Manuscript **Received** December 21, 2000; **Revised** October 17, 2001)

1. Introduction

In recent years, parallel manipulators have drawn much attention due to their desirable characteristics such as high rigidity and low error accumulation. Parallel manipulators are composed of closed chains, which enhance the stiffness and positioning accuracy but can complicate the kinematic and dynamic characteristics. Nevertheless, the kinematic and dynamic analyses are very

important for their design and control since the accurate dynamic model, and the consequent knowledge of the dynamic characteristics of parallel manipulators enable designers to devise an efficient controller design for high-speed operations.

The traditional Newton-Euler approach for serial manipulators are composed of forward and backward recursions. The motion of each link is derived through forward recursion, and Newton-Euler equations are derived through backward recursion. However, in the case of parallel manipulators, because of closed chain kinematic architectures, the independent forward and backward computations are impossible. Therefore, a computation technique that is unique to each closed chain architecture needs to be developed.

Lebret et al. derived dynamic equations of a simple Stewart platform (UPS type: In this paper, the bar underneath the capital letter (e. g. P) signifies the actuated joint.) by the Lagrangian approach. Revoulet and Berthomieu derived the inverse dynamic equations of a Stewart platform by the Newton-Euler approach neglecting the Coriolis, centrifugal terms. Dasgupta and Mruthyunjaya derived inverse dynamic equations of a Stewart platform by the same approach while considering joint frictions as well as link inertia effects. Miller used the Hamilton's principle, Codourey used the virtual work theory, and Kim et al. used Kane's methods in their derivation of equations of motion of DELTA robots. Ji studied leg inertia effect through the decoupled leg dynamic equations of a Stewart platform. Gosselin derived inverse dynamics of a Stewart platform by the Newton-Euler approach and discussed parallel computational algorithm. Dasgupta and Choudhury presented a general strategy based on the Newton-Euler approach to the dynamic formulation of parallel manipulators. They derived the dynamic equations for six planar and spatial (PRPS, RRRS, RPS type) types of parallel manipulators.

In the Newton-Euler approach, however, the way of deriving equations of motion as well as the derived equations depend on the specific kinematic architecture of the mechanism. This paper presents inverse kinematic and dynamic equations of 6-DOF PUS HexaSlide type parallel manipulators through the Newton-Euler approach. The equations include the link inertia and joint frictions in all joints, the relative importance of which are investigated by computer simulation.

The 6-DOF PUS HexaSlide type parallel manipulator (HSM) is composed of 6 sliding actuators, 6 fixed length links, and a mobile platform. The sliders move along linear motion guides that are fixed on the ground. The links are of constant length and are connected to the sliders through universal joints (U). The axes of the prismatic joints along which the centers of the universal joints are being translated will be referred to as the rail axes. Finally, the links are connected to the mobile platform through spherical joints (S). The several known examples of 6-DOF robots that fall into this group are the "Hexaglide" robot at ETH Zurich [Fig. 1.3(a)], the "HexaM" milling machine by Toyoda [Fig. 1. 3(b)], the "active wrist" proposed by Merlet and Gosselin [Fig. 1.3(c)]. The HSMs have many attractive characteristics such as fixed actuators and lighter moving parts compared to the parallel manipulators with moving actuators, among others. To the best of our knowledge, however, there has not been any research on the dynamics of HSM. It is probably due to the fact that their analysis is generally more complicated than the analysis of the other simpler types of parallel manipulators such as Stewart platforms.

The paper is organized as follows: In the next section, inverse kinematic analyses are presented. In the kinematic analyses, the kinematic motion (posture, velocity, acceleration) of each slider, link, and platform as well as articular variable are derived for a given desired trajectory of a platform. In Sec. 3, Newton and Euler equations are constructed for each body using the kinematic motion information. From these equations, inverse dynamic equations of HSM are derived. In Sec. 4, the accuracy of the derived dynamic model is compared against that of another model that is generated by a fully nonlinear dynamic analysis software. In addition, relative importance

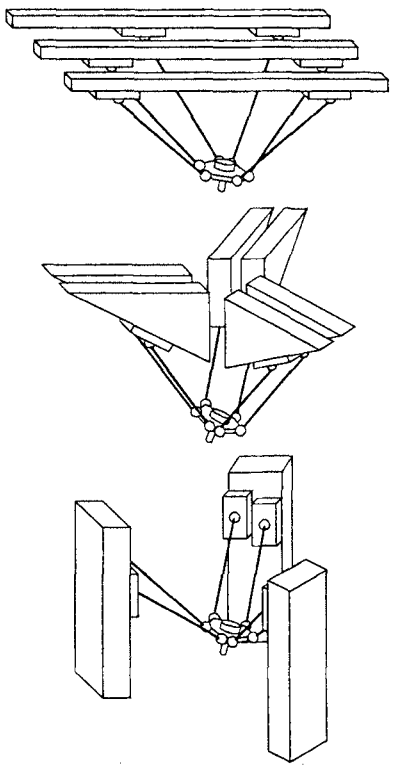

Fig. 1 Three examples of HSMs: (a) the "Hexaglide" robot, (b) the "HexaM" machine, and (c) a similar model of the "active wrist"

of the link inertia and joint frictions on the computed torque is investigated. Finally, in the last section, conclusions of the present work are summarized.

2. Inverse Kinematic Analysis of the Model

In order to derive the Newton-Euler equations of sliders, links, and platform, the motion of each body is needed. Through the inverse kinematics, the motion of each body can be determined given the desired trajectory of the mobile platform. In the general HSM (Fig. 2), the start and end points of rail axis i ($i=1, 2, ..., 6$) will be denoted respectively by $\mathbf{A}_{i,0}$ and $\mathbf{A}_{i,1}$. The center of universal joint i, which lies on the line segment $\mathbf{A}_{i,0}\mathbf{A}_{i,1}$(rail axis i), will be denoted by a base joint $\mathbf{A}_i$. A right-handed base reference frame with

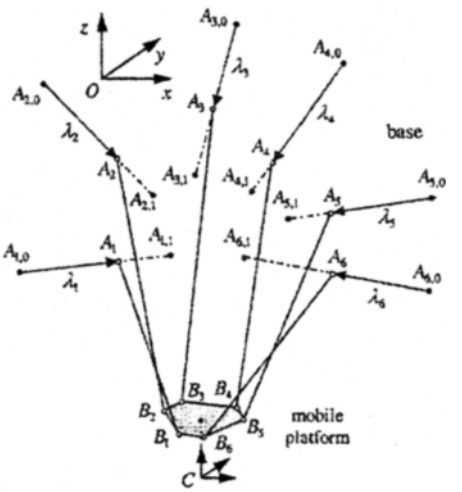

Fig. 2 Schematic diagram of hexaSlide manipulator

center **O** is attached to the base. The center of spherical joint i will be denoted by a platform joint $\mathbf{B}_i$. The mobile reference frame is attached to the mobile platform at the tool tip point **C**. The distance between points $\mathbf{A}_{i,0}$ and $\mathbf{A}_i$ will be denoted by articular coordinate λ_i. Changing the values of the articular coordinates will control the posture of the mobile platform.

2.1 Platform

The position of the platform is denoted by point **C** measured from the origin **O**, and the orientation is expressed by three Euler angles $[\Psi\ \theta\ \phi]$. The position and orientation are prescribed through desired path planning. For convenience, three successive Euler angles are defined as follows: First rotate about the base X axis by the angle Ψ. Next rotate about the base Y axis by the angle θ. Finally rotate about the mobile z axis by the angle ϕ. In this case, the orientation matrix (**R**) of the platform is given by

$$\mathbf{R}=\mathbf{R}_{Y,\theta}\mathbf{R}_{X,\Psi}\mathbf{R}_{Z,\phi}$$

$$=\begin{bmatrix} C\theta & 0 & S\theta \\ 0 & 1 & 0 \\ -S\theta & 0 & C\theta \end{bmatrix}\begin{bmatrix} 1 & 0 & 0 \\ 0 & C\Psi & -S\Psi \\ 0 & S\Psi & C\Psi \end{bmatrix}\begin{bmatrix} C\phi & -S\phi & 0 \\ S\phi & C\phi & 0 \\ 0 & 0 & 1 \end{bmatrix} \quad (1)$$

$$=\begin{bmatrix} C\theta C\phi+S\Psi S\theta S\phi & -C\theta S\phi+S\Psi S\theta C\phi & C\Psi S\theta \\ C\Psi S\phi & C\Psi C\phi & -S\Psi \\ -S\theta C\phi+S\Psi C\theta S\phi & S\theta S\phi+S\Psi C\theta C\phi & C\Psi C\theta \end{bmatrix}$$

where $C\theta$ and $S\theta$ represent $\cos\theta$ and $\sin\theta$, respectively.

The translational velocity and acceleration of the platform are derived directly by taking time differentiation of the position vector. For deriving the angular velocity, the relations $\dot{\mathbf{R}}=\omega^{\times}\mathbf{R}$ between the orientation matrix($\mathbf{R}$) and the angular velocity(ω) are used. Here, $\omega^{\times}$ denotes a skew-symmetric matrix generated by ω. Then, the angular velocity and angular acceleration of the platform are derived as

$$\boldsymbol{\omega}=\begin{bmatrix}\dot{\Psi}C\theta+\dot{\phi}S\theta C\Psi\\ \dot{\theta}-\dot{\phi}S\Psi\\ -\dot{\Psi}S\theta+\dot{\phi}C\theta C\Psi\end{bmatrix} \tag{2}$$

$$\boldsymbol{\omega}=\begin{bmatrix}\ddot{\Psi}C\theta-\dot{\theta}\dot{\Psi}S\theta+\ddot{\phi}S\theta C\Psi-\dot{\phi}\dot{\Psi}S\theta S\Psi+\dot{\phi}\dot{\theta}C\theta C\Psi\\ \ddot{\theta}-\ddot{\phi}S\Psi-\dot{\phi}\dot{\Psi}C\Psi\\ -\ddot{\Psi}S\theta-\dot{\Psi}\dot{\theta}C\theta+\ddot{\phi}C\theta C\Psi-\dot{\phi}\dot{\theta}S\theta C\Psi-\dot{\phi}\dot{\Psi}C\theta S\Psi\end{bmatrix} \tag{3}$$

In order to derive the motion of the sliders and links and dynamic equations of the platform in the later sections, motion of $\mathbf{B}_i$ and $\mathbf{G}$ (center of gravity of the platform) are derived as follows:

$$\begin{aligned}\mathbf{B}_i&=\mathbf{C}+\mathbf{RCB}_i'\\ \dot{\mathbf{B}}_i&=\dot{\mathbf{C}}+\boldsymbol{\omega}^{\times}\mathbf{RCB}_i'\\ \ddot{\mathbf{B}}_i&=\ddot{\mathbf{C}}+(\dot{\boldsymbol{\omega}}^{\times}+\boldsymbol{\omega}^{\times}\boldsymbol{\omega}^{\times})\,\mathbf{RCB}_i'\end{aligned} \tag{4}$$

$$\begin{aligned}\mathbf{G}&=\mathbf{C}+\mathbf{RCG}'\\ \dot{\mathbf{G}}&=\dot{\mathbf{C}}+\bar{\omega}\mathbf{RCG}'\\ \ddot{\mathbf{G}}&=\ddot{\mathbf{C}}+(\dot{\boldsymbol{\omega}}^{\times}+\boldsymbol{\omega}^{\times}\boldsymbol{\omega}^{\times})\,\mathbf{RCG}'\end{aligned} \tag{5}$$

where the constant $\mathbf{CB}_i'$ and $\mathbf{CG}'$ vectors ar e expressed in the platform reference frame.

2.2 Slider

Kinematic analysis of the slider involves computing the articular variable (λ_i) when the slider is moving on a linear guide from point $\mathbf{A}_{i,0}$. Figure 3 shows a detailed kinematic model of the slider part. Let $\mathbf{a}_i$ be the unit vector along the rail axis $\mathbf{A}_{i,0}\mathbf{A}_{i,1}$. Based on the HSM geometry, the following equations are derived:

$$\mathbf{A}_i\mathbf{B}_i=\mathbf{A}_{i,0}\mathbf{B}_i-\mathbf{A}_{i,0}\mathbf{A}_i=\mathbf{d}_i-\lambda_i\mathbf{a}_i \tag{6}$$

Since the vector $\mathbf{A}_i\mathbf{B}_i$ has the constant magnitude l, the following equations are derived:

$$(\mathbf{d}_i-\lambda_i\mathbf{a}_i)^{\mathrm{T}}(\mathbf{d}_i-\lambda_i\mathbf{a}_i)=l^2 \tag{7}$$

Solving Eq. (7) for the articular variable (λ_i)

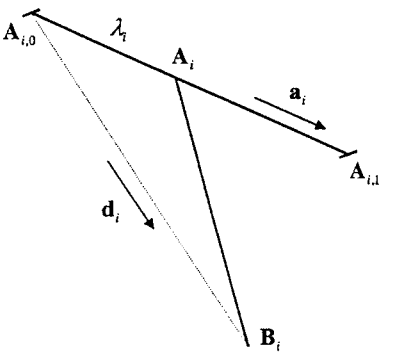

Fig. 3 Kinematic model of slider and link

and taking only the physically meaningful value from the two solutions, we obtain:

$$\lambda_i=\mathbf{a}_i^{\mathrm{T}}\mathbf{d}_i-\sqrt{(\mathbf{a}_i^{\mathrm{T}}\mathbf{d}_i)^2-\mathbf{d}_i^{\mathrm{T}}\mathbf{d}_i+l^2} \tag{8}$$

Therefore λ_i is obtained by knowing $\mathbf{d}_i$ vector (i.e. $\mathbf{B}_i$ from Eq. (4)). The velocity and acceleration of λ_i can be obtained by direct differentiation of Eq. (8) as

$$\dot{\lambda}_i=\mathbf{a}_i^{\mathrm{T}}\dot{\mathbf{d}}_i-\frac{\dot{k}(t)}{2\sqrt{k(t)}} \tag{9}$$

$$\ddot{\lambda}_i=\mathbf{a}_i^{\mathrm{T}}\ddot{\mathbf{d}}-\frac{(2\dot{k}(t)\,k(t)-\dot{k}(t)^2)}{4k(t)\sqrt{k(t)}} \tag{10}$$

$$\begin{aligned}&\textit{where } k(t)=(\mathbf{a}_i^{\mathrm{T}}\mathbf{d}_i)^2-\mathbf{d}_i^{\mathrm{T}}\mathbf{d}_i+l^2,\\ &\qquad \dot{k}(t)=2(\mathbf{a}_i^{\mathrm{T}}\mathbf{d}_i)\,(\mathbf{a}_i^{\mathrm{T}}\dot{\mathbf{d}}_i)-2\mathbf{d}_i^{\mathrm{T}}\dot{\mathbf{d}}_i\\ &\qquad \ddot{k}(t)=2(\mathbf{a}_i^{\mathrm{T}}\dot{\mathbf{d}}_i)^2+2(\mathbf{a}_i^{\mathrm{T}}\mathbf{d}_i)\,(\mathbf{a}_i^{\mathrm{T}}\ddot{\mathbf{d}}_i)\\ &\qquad\qquad -2\dot{\mathbf{d}}_i^{\mathrm{T}}\dot{\mathbf{d}}_i-2\mathbf{d}_i^{\mathrm{T}}\ddot{\mathbf{d}}_i\end{aligned}$$

Note that these expressions are quite complex due to the square root term. However, in the case of the Stewart platform, inverse kinematic solution is simply $\lambda_i=\|\mathbf{A}_i\mathbf{B}_i\|$, where point $\mathbf{A}_i$ is fixed to the base, which simplifies kinematic and dynamic analyses. The more complicated inverse kinematic solution of the HSM will render all other analyses much more complicated.

For the link kinematic analysis and inverse dynamic analysis in the next section, the motion of point $\mathbf{A}_i$ should be given as follows:

$$\mathbf{A}_i=\mathbf{A}_{i,0}+\lambda_i\mathbf{a}_i,\ \dot{\mathbf{A}}_i=\dot{\lambda}_i\mathbf{a}_i,\ \ddot{\mathbf{A}}_i=\ddot{\lambda}_i\mathbf{a}_i \tag{11}$$

2.3 Link

Let $\mathbf{n}_i$ be the unit vector along the i-th link length direction (i.e. $\mathbf{n}_i=(\mathbf{B}_i-\mathbf{A}_i)/l$) and point $\mathbf{P}_i$ be the gravity center position of the link. The translational motion of a link can easily be

derived as

$$\mathbf{P}_i=\mathbf{A}_{i,0}+\lambda_i\mathbf{a}_i+\frac{l}{2}\mathbf{n}_i,\ \dot{\mathbf{P}}_i=\dot{\lambda}_i\mathbf{a}_i+\frac{l}{2}\dot{\mathbf{n}}_i,$$
$$\ddot{\mathbf{P}}_i=\ddot{\lambda}_i\mathbf{a}_i+\frac{l}{2}\ddot{\mathbf{n}}_i \tag{12}$$

Next, consider the rotational motion of a link. Since each link of the HSM is composed of a universal-spherical joint pair, it has 2 DOF rotational motion. The universal joint has two rotational axes. One is attached to the link and the other is attached to the slider. Let the axis attached to the slider be $\boldsymbol{\alpha}_i$ and the axis attached to the link be $\boldsymbol{\beta}_i$. In the case of a general universal joint, $\boldsymbol{\beta}_i$ is perpendicular to $\boldsymbol{\alpha}_i$ as well as to $\mathbf{n}_i$. A reference frame of the link is attached to the center of the link, with axis defined along the $\mathbf{n}_i$ vector, and y axis is along the $\boldsymbol{\beta}_i$ vector, and x axis defined by the right hand rule. Hence the rotation matrix of a link is derived as

$$\mathbf{R}_{li}=\left[\frac{(\mathbf{n}_i\times\boldsymbol{\alpha}_i)\times\mathbf{n}_i}{\|\mathbf{n}_i\times\boldsymbol{\alpha}_i\|}\quad\frac{\mathbf{n}_i\times\boldsymbol{\alpha}_i}{\|\mathbf{n}_i\times\boldsymbol{\alpha}_i\|}\mathbf{n}_i\right] \tag{13}$$

Note that the axis $\boldsymbol{\alpha}_i$ is a fixed axis. Thus, the configuration-dependent moment of inertia of the link is derived as

$$\mathbf{I}_{li}=\mathbf{R}_{li}\mathbf{I}'_{li}\mathbf{R}_{li}^T \tag{14}$$

where $\mathbf{I}'_{li}$ is the constant moment of inertia about the link local coordinate frame.

The angular velocity of the link ($\boldsymbol{\omega}_{li}$) can be computed exactly from Eq. by using the relationship $\boldsymbol{\omega}_{li}^{\times}=\dot{\mathbf{R}}_{li}\mathbf{R}_{li}^T$. However, this direct computation may lead to very complicated expressions for $\boldsymbol{\omega}_{li}$ and $\dot{\boldsymbol{\omega}}_{li}$. If the parallel manipulator has slender links and is not moving fast, the kinetic energy of the link associated with the rotation about the link direction ($\mathbf{n}_i$) may be negligible. In this case, the angular velocity of the link can be derived with great simplification as follows:

The angular velocity of the link is related to $\dot{\mathbf{n}}_i$. This fact can be shown in the following equations:

$$\dot{\mathbf{B}}_i=\dot{\mathbf{A}}_i+l\dot{\mathbf{n}}_i=\dot{\mathbf{A}}_i+\boldsymbol{\omega}_{li}^{\times}(l\mathbf{n}_i) \tag{15}$$

Rearranging Eq. (15) leads to

$$\mathbf{n}_i^{\times}\boldsymbol{\omega}_{li}=-\dot{\mathbf{n}}_i \tag{16}$$

Using the mathematical relation $\mathbf{I}_{3\times3}+\mathbf{n}_i^{\times}\mathbf{n}_i^{\times}=\mathbf{n}_i\mathbf{n}_i^T$, the angular velocity of a link can be expressed as

$$\boldsymbol{\omega}_{li}+\mathbf{n}_i^{\times}\mathbf{n}_i^{\times}\boldsymbol{\omega}_{li}=\mathbf{n}_i\mathbf{n}_i^T\boldsymbol{\omega}_{li} \tag{17}$$

In the slowly rotating slender link case, the angular velocity about the link length direction may be negligible, i.e. $\mathbf{n}_i^T\boldsymbol{\omega}_{li}\approx0$. Thus, Eq. (17) can be rewritten as

$$\mathbf{n}_i^{\times}\mathbf{n}_i^{\times}\boldsymbol{\omega}_{li}=-\boldsymbol{\omega}_{li} \tag{18}$$

Multiplying $\mathbf{n}_i^{\times}$ to both sides of Eq. (16) gives $\mathbf{n}_i^{\times}\mathbf{n}_i^{\times}\boldsymbol{\omega}_{li}=-\mathbf{n}_i^{\times}\dot{\mathbf{n}}_i(=-\boldsymbol{\omega}_{li}$ from Eq. (18)). Therefore, the following simplified equations for the angular velocities and accelerations are derived as

$$\begin{aligned}\boldsymbol{\omega}_{li}&=\mathbf{n}_i^{\times}\dot{\mathbf{n}}_i\\ \dot{\boldsymbol{\omega}}_{li}&=\dot{\mathbf{n}}_i^{\times}\dot{\mathbf{n}}_i+\mathbf{n}_i^{\times}\ddot{\mathbf{n}}_i=\mathbf{n}_i^{\times}\ddot{\mathbf{n}}_i\end{aligned} \tag{19}$$

since $\dot{\mathbf{n}}_i^{\times}\dot{\mathbf{n}}_i=0$.

3. Inverse Dynamic Analysis of the Model

The motion of the sliders, links, and platform are derived through inverse kinematic analyses of each body in the previous chapter. Then, Newton-Euler equations of each body can be constructed to derive the inverse dynamic equations which determine the required actuator force when the desired platform motion is prescribed.

3.1 Slider

In the slider body, there are the gravity force, actuator force, reaction force at point $\mathbf{A}_i$, and reaction/friction forces from the linear guide. Thus, the Newton equations of motion of the slider body is constructed as (see Fig. 4)

$$\tau_i\mathbf{a}_i+m_{si}\mathbf{g}+\mathbf{N}_i+f_{si}\mathbf{a}_i-\mathbf{F}_{Ai}=m_{si}\ddot{\lambda}_i\mathbf{a}_i \tag{20}$$

where τ_i is the actuator force to be computed, m_{si} is the i-th slider mass, $\mathbf{N}_i$ is the normal reaction force between the slider and the linear guide, f_{si} is the friction force by the linear guide, and $\mathbf{F}_{Ai}$ is the reaction force at point $\mathbf{A}_i$. The friction force model is considered in Sec. 3.4. The actuating force (τ_i) can be obtained by taking the dot products involving the $\mathbf{a}_i$ vector, and the normal

force ($\mathbf{N}_i$) has the $\mathbf{u}_i$ and $\mathbf{v}_i$ components Thus,

$$\begin{aligned}\tau_i &= m_{Si}\ddot{\lambda}_i - f_{Si} - m_{Si}(\mathbf{a}_i^T\mathbf{g}) + \mathbf{a}_i^T\mathbf{F}_{Ai} \\ \mathbf{N}_i &= (\mathbf{u}_i^T\mathbf{F}_{Ai} - m_{Si}\mathbf{u}_i^T\mathbf{g})\,\mathbf{u}_i + (\mathbf{v}_i^T\mathbf{F}_{Ai} - m_{Si}\mathbf{v}_i^T\mathbf{g})\,\mathbf{v}_i\end{aligned} \tag{21}$$

In order to compute the actuator and normal forces, the reaction force $\mathbf{F}_{Ai}$ at point $\mathbf{A}_i$ should be obtained by the dynamic analyses of the link and platform bodies described in the following sections.

3.2 Link

In the link part, there are the gravity force, reaction force from the slider ($\mathbf{F}_{Ai}$), reaction force from the platform ($\mathbf{F}_{Bi}$), transmitted frictional moment through the universal joint ($\mathbf{M}_{Ai}$), universal joint friction moment ($\mathbf{f}_{ui}$), and spherical joint friction moment ($\mathbf{f}_{pi}$). Thus, the Newton-Euler equations of motion of the link part is constructed as (see Fig. 5)

$$\begin{aligned}&\mathbf{F}_{Ai} + \mathbf{F}_{Bi} + m_{li}\mathbf{g} = m_{li}\ddot{\lambda}_i\mathbf{a}_i + m_{li}\frac{l}{2}\ddot{\mathbf{n}}_i \\ &\frac{l}{2}\mathbf{n}_i^{\times}(\mathbf{F}_{Bi} - \mathbf{F}_{Ai}) + \mathbf{f}_{ui} + \mathbf{f}_{pi} + \mathbf{M}_{Ai} = \mathbf{I}_{li}\dot{\boldsymbol{\omega}}_{li} + \boldsymbol{\omega}_{li}^{\times}(\mathbf{I}_{li}\boldsymbol{\omega}_{li})\end{aligned} \tag{22}$$

From Eqs. (19) and (22), the following equation is derived:

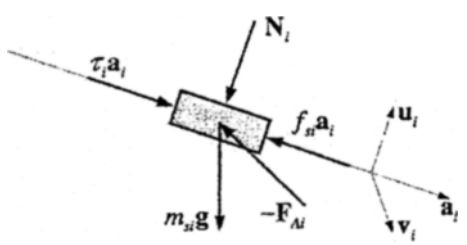

Fig. 4 The detailed dynamic model of slider part

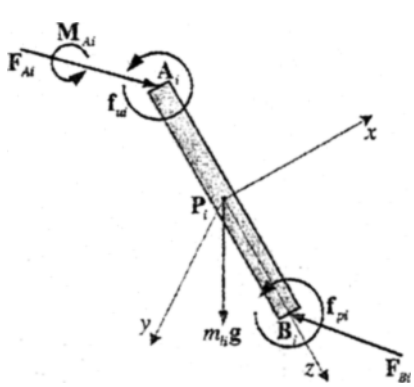

Fig. 5 The detailed dynamic model of link part

$$\begin{aligned}\mathbf{n}_i^{\times}\mathbf{F}_{Bi} = &\frac{1}{2}m_{li}\ddot{\lambda}_i\mathbf{n}_i^{\times}\mathbf{a}_i - \frac{1}{2}m_{li}\mathbf{n}_i^{\times}\mathbf{g} + \frac{1}{l}\boldsymbol{\omega}_{li}^{\times}(\mathbf{I}_{li}\boldsymbol{\omega}_{li}) \\ &+ \frac{1}{l}\left(\mathbf{I}_{li} + m_{li}\left(\frac{l}{2}\right)^2\mathbf{I}_{3\times3}\right)\dot{\boldsymbol{\omega}}_{li} + \frac{1}{l}\mathbf{f}_{ui} \\ &- \frac{1}{l}\mathbf{f}_{pi} - \frac{1}{l}\mathbf{M}_{Ai}\end{aligned} \tag{23}$$

Then, through the mathematical relation $\mathbf{I}_{3\times3}\mathbf{n}_i^{\times}\mathbf{n}_i^{\times} = \mathbf{n}_i\mathbf{n}_i^T - \mathbf{I}$, $\mathbf{F}_{Bi}$ can be expressed as

$$\mathbf{F}_{Bi} = -\mathbf{n}_i^{\times}\mathbf{n}_i^{\times}\mathbf{F}_{Bi} + F'_{Biz}\mathbf{n}_i \tag{24}$$

where $F'_{Biz} = \mathbf{n}_i^T\mathbf{F}_{Bi}$ is the component of $\mathbf{F}_{Bi}$ on the slider axis. The term $\mathbf{n}_i^{\times}\mathbf{n}_i^{\times}\mathbf{F}_{Bi}$ can be calculated by Eq. (23). Note in this computation process that $\mathbf{M}_{Ai}$ is eliminated through the cross-product with the unit vector $\mathbf{n}_i$ because $\mathbf{M}_{Ai}$ has only the $\mathbf{n}_i$ direction component. This is because the universal joint has only rotational constraint about $\mathbf{n}_i$ direction. However, the term $F'_{Biz}\mathbf{n}_i$ cannot be evaluated in the link part only. Therefore the computation of $F'_{Biz}\mathbf{n}_i$ requires the dynamic analysis of the platform part, which is explained in the next section.

3.3 Platform

In the platform part, there are the gravity force, reaction force from the link ($\mathbf{F}_{Bi}$), spherical joint friction ($\mathbf{f}_{pi}$), and the externally applied force ($\mathbf{f}(t)$) and moment ($\mathbf{M}(t)$). Thus, the Newton-Euler equations of motion of the platform part are constructed as (See Fig. 6)

$$\begin{aligned}&m\mathbf{g} + \mathbf{f}(t) - \Sigma\mathbf{F}_{Bi} = m\ddot{\mathbf{C}} + m\dot{\boldsymbol{\omega}}^{\times}\mathbf{RCG}' + m\boldsymbol{\omega}^{\times}\boldsymbol{\omega}^{\times}\mathbf{RCG}' \\ &\mathbf{M}(t) + \mathbf{GT}^{\times}\mathbf{f}(t) - \Sigma\mathbf{f}_{pi} - \Sigma\mathbf{GB}_i^{\times}\mathbf{F}_{Bi} = \mathbf{I}\dot{\boldsymbol{\omega}} + \boldsymbol{\omega}^{\times}\mathbf{I}\boldsymbol{\omega}\end{aligned} \tag{25}$$

Let γ_i be a 1×6 row vector composed of o's except for the i-th element with the value of 1. Then, from Eq. (25) the F'_{Biz} component can be derived when the $\mathbf{T}_1$ matrix is invertible as

$$F'_{Biz} = \gamma_i\mathbf{T}_1^{-1}\mathbf{T} \tag{26}$$

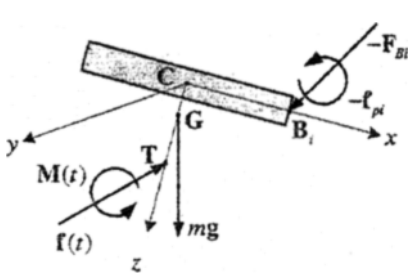

Fig. 6 The detailed dynamic model of platform part

where

$$\mathbf{T}=\begin{bmatrix} mg-m\ddot{\mathbf{G}}+\mathbf{f}(t)+\Sigma\mathbf{n}_i^{\times}\mathbf{n}_i^{\times}\mathbf{F}_{Bi} \\ -\mathbf{I}\dot{\boldsymbol{\omega}}-\boldsymbol{\omega}^{\times}\mathbf{I}\boldsymbol{\omega}+\mathbf{M}(t)+\mathbf{G}\mathbf{T}^{\times}\mathbf{f}(t)+\Sigma\mathbf{G}\mathbf{B}_i^{\times}\mathbf{n}_i^{\times}\mathbf{n}_i^{\times}\mathbf{F}_{Bi}-\Sigma\mathbf{f}_{pi} \end{bmatrix}$$

$$\mathbf{T}_1=\begin{bmatrix} \mathbf{n}_1 & \mathbf{n}_2 & \mathbf{n}_3 & \mathbf{n}_4 & \mathbf{n}_5 & \mathbf{n}_6 \\ \mathbf{GB}_1^{\times}\mathbf{n}_1 & \mathbf{GB}_2^{\times}\mathbf{n}_2 & \mathbf{GB}_3^{\times}\mathbf{n}_3 & \mathbf{GB}_4^{\times}\mathbf{n}_4 & \mathbf{GB}_5^{\times}\mathbf{n}_5 & \mathbf{GB}_6^{\times}\mathbf{n}_6 \end{bmatrix}$$

Thus, $\mathbf{F}_{Bi}$ is derived from Eqs. (23), (24), and (26) as

$$\begin{aligned}\mathbf{F}_{Bi}=&-\frac{1}{l}\mathbf{n}_i^{\times}\left(\mathbf{I}_{li}+m_{li}\left(\frac{l}{2}\right)^2\mathbf{I}_{3\times3}\right)\dot{\boldsymbol{\omega}}_{li}\\&-\frac{1}{l}\mathbf{n}_i^{\times}\boldsymbol{\omega}_{li}^{\times}(\mathbf{I}_{li}\boldsymbol{\omega}_{li})+\frac{1}{l}\mathbf{n}_i^{\times}\mathbf{f}_{ui}+\frac{1}{l}\mathbf{n}_i^{\times}\mathbf{f}_{pi}\\&-\frac{1}{2}m_{li}\bar{\lambda}_i\mathbf{n}_i^{\times}\mathbf{n}_i^{\times}\mathbf{a}_i+\frac{1}{2}m_{li}\mathbf{n}_i^{\times}\mathbf{n}_i^{\times}\mathbf{g}+\mathbf{n}_i\gamma_i\mathbf{T}_1^{-1}\mathbf{T}\end{aligned}\tag{27}$$

Then, by Eq. (22), $\mathbf{F}_{Ai}$ is derived as

$$\begin{aligned}\mathbf{F}_{Ai}=&\frac{1}{l}\mathbf{n}_i^{\times}\mathbf{I}_{li}\dot{\boldsymbol{\omega}}_{li}+\frac{1}{l}\mathbf{n}_i^{\times}\boldsymbol{\omega}_{li}^{\times}(\mathbf{I}_{li}\boldsymbol{\omega}_{li})-\frac{1}{l}\mathbf{n}_i^{\times}\mathbf{f}_{ui}\\&-\frac{1}{l}\mathbf{n}_i^{\times}\mathbf{f}_{pi}+\frac{l}{2}m_{li}(\mathbf{I}_{3\times3}+\mathbf{n}_i\mathbf{n}_i^T)\ddot{\mathbf{n}}_i\\&+\frac{1}{2}m_{li}\bar{\lambda}(\mathbf{I}_{3\times3}+\mathbf{n}_i\mathbf{n}_i^T)\mathbf{a}_i\\&-\frac{1}{2}m_{li}(\mathbf{I}_{3\times3}+\mathbf{n}_i\mathbf{n}_i^T)\mathbf{g}-\mathbf{n}_i\gamma_i\mathbf{T}_1^{-1}\mathbf{T}\end{aligned}\tag{28}$$

Finally, the inverse dynamic equation for computing required actuator force τ_i is derived by Eq. (21) as

$$\begin{aligned}\tau_i=&m_{si}(\ddot{\lambda}_i-\mathbf{a}_i^T\mathbf{g})-f_{si}+\frac{1}{l}\mathbf{a}_i^T\mathbf{n}_i^{\times}\mathbf{I}_{li}\dot{\boldsymbol{\omega}}_{li}\\&+\frac{1}{l}\mathbf{a}_i^T\mathbf{n}_i^{\times}\boldsymbol{\omega}_{li}^{\times}(\mathbf{I}_{li}\boldsymbol{\omega}_{li})-\frac{1}{l}\mathbf{a}_i^T\mathbf{n}_i^{\times}\mathbf{f}_{ui}-\frac{1}{l}\mathbf{a}_i^T\mathbf{n}_i^{\times}\mathbf{f}_{pi}\\&+\frac{l}{4}m_{li}\mathbf{a}_i^T(\mathbf{I}_{3\times3}+\mathbf{n}_i\mathbf{n}_i^T)\ddot{\mathbf{n}}_i+\frac{1}{2}m_{li}\bar{\lambda}_i\mathbf{a}_i^T(\mathbf{I}_{3\times3}\\&+\mathbf{n}_i\mathbf{n}_i^T)\mathbf{a}_i-\frac{1}{2}m_{li}\mathbf{a}_i^T(\mathbf{I}_{3\times3}+\mathbf{n}_i\mathbf{n}_i^T)\mathbf{g}\\&-\mathbf{a}_i^T\mathbf{n}_i\gamma_i\mathbf{T}_1^{-1}\mathbf{T}\end{aligned}\tag{29}$$

The right side of Eq. (29) is calculated through the inverse kinematic analysis presented in Section 2. Note that $\mathbf{a}_i^T\mathbf{n}_i\gamma_i\mathbf{T}_1^{-1}$ is related to the kinematic Jacobian matrix and the $\mathbf{T}$ matrix shows coupled dynamic effects between the platform part and link parts in the parallel manipulators because of the closed chain architectures.

In the mechanical design, we need the joint reaction forces and moments that are easily computed by Eq. (21) for $\mathbf{N}_i$, by Eq. (27) for spherical joint $\mathbf{F}_{Bi}$, and by Eq. (28) for universal joint $\mathbf{F}_{Ai}$. The reaction moment at the universal joint can also be computed from Eq. (23).

3.4 Friction modeling

For more accurate position control and dynamic simulation, appropriate friction models in the linear slide guide, ball screws, and in the universal and spherical joints should be incorporated in the dynamic equations of motion. First, friction force (f_{si}) in the slider part can be modeled as follows:

$$f_{si}=-c_{si}\dot{\lambda}_i-\mu_{si}(\mathbf{u}_i^T-\mathbf{v}_i^T)\mathbf{N}_i sign(\dot{\lambda}_i)-\tau_b/pitch\tag{30}$$

where c_{si}, μ_{si}, τ_b, and pitch denote the viscous friction coefficient, coulomb friction coefficient, frictional moment by the internal pressure in the ball screw, and pitch of the screw respectively. Second, frictional moments in the universal and spherical joints can be modeled by:

$$\begin{aligned}\mathbf{f}_{ui}&=-c_{ui}\boldsymbol{\omega}_{li}-\tau_{ui}\\\mathbf{f}_{pi}&=-c_{pi}(\boldsymbol{\omega}_{li}-\boldsymbol{\omega})-\tau_{pi}\end{aligned}\tag{31}$$

where c_{ui}, c_{pi}, τ_{ui}, and τ_{pi} are viscous friction coefficients and static frictional moments in the universal and spherical joints, respectively. Note that the static frictional moments have the same direction as the viscous frictional moments since the frictional moments act opposite to the rotational direction.

The actuation forces needed to overcome those frictional moments in Eq. (31) are written as

$$\boldsymbol{\tau}_{fui}=-\frac{1}{l}\mathbf{a}_i^T\mathbf{n}_i^{\times}\mathbf{f}_{ui}-\mathbf{a}_i^T\mathbf{n}_i\gamma_i\mathbf{T}_1^{-1}\begin{bmatrix} -\Sigma\frac{1}{l}\mathbf{n}_i^{\times}\mathbf{f}_{ui} \\ -\Sigma\frac{1}{l}\mathbf{G}\mathbf{B}_i^{\times}\mathbf{n}_i^{\times}\mathbf{f}_{ui}\end{bmatrix}$$

$$\boldsymbol{\tau}_{fpi}=-\frac{1}{l}\mathbf{a}_i^T\mathbf{n}_i^{\times}\mathbf{f}_{pi}-\mathbf{a}_i^T\mathbf{n}_i\gamma_i\mathbf{T}_1^{-1}\begin{bmatrix} -\Sigma\frac{1}{l}\mathbf{n}_i^{\times}\mathbf{f}_{pi} \\ -\Sigma\frac{1}{l}\mathbf{G}\mathbf{B}_i^{\times}\mathbf{n}_i^{\times}\mathbf{f}_{pi}-\Sigma\mathbf{f}_{pi}\end{bmatrix}\tag{32}$$

4. Effects of Link Inertia and Joint Friction

In order to improve control performance, it is necessary to fully understand dynamic characteristics. The inverse dynamic equation of

HSM (Eq. (29)) is very complex and requires much calculation time. Therefore, we may ignore less important dynamic terms for rapid real-time calculation in situations involving slow motion or small applied end-effector forces. In this section, therefore, relative importance of the joint friction and link inertia effects are analyzed by computer simulation for typical operations. The geometrical and dynamic parameters of the HSM for computer simulation are summarized in Appendix I.

4.1 Accuracy of dynamic model

In order to verify the correctness of the derived inverse dynamic equations of a HSM, computer simulation has been performed. In this simulation, a commercial dynamic analysis software, DADS (Dynamic Analysis and Design System), is used in order to get the reference results. First, an inverse dynamic analysis of a 3D model of the HSM in DADS computes the actuator forces given desired trajectory of a platform. Then, the derived inverse dynamic equations coded in MATLAB generate actuator forces. In the following simulation cases, the frictional effects are not considered because it is difficult to measure true friction parameters and because it is difficult to implement friction models in DADS.

Figure 7 shows the actuator forces when the desired trajectory of the platform is given as a constant radius circular motion (r=100mm) with a speed of 40 rpm. Figure 8 shows the actuator forces for another desired trajectory of the platform that is moving with a constant acceleration (Eq. (33): translational accelerations are in [m/sec^2], angular accelerations are in [rad/sec^2]).

$$\ddot{X}=\begin{Bmatrix}[0.1\ 0.1\ 0.1\ 0.05\ 0.05\ 0.1]^T, \text{ for } 0\le t\le 1.5s\\ [-0.1\ -0.1\ -0.1\ -0.05\ -0.05\ -0.1]^T, \text{ for } 1.5\le t\le 3s\end{Bmatrix} \quad (33)$$

As shown in Figs. 7 and 8, the MATLAB simulation results are almost the same as DADS results. A minor discrepancy between the MATLAB and DADS results may be due to the simplified slender link model. We simulated other desired trajectories with higher speeds, which also showed good agreement with two simulation results. The simulation results, therefore, validate the correctness of the derived equations for the most cases.

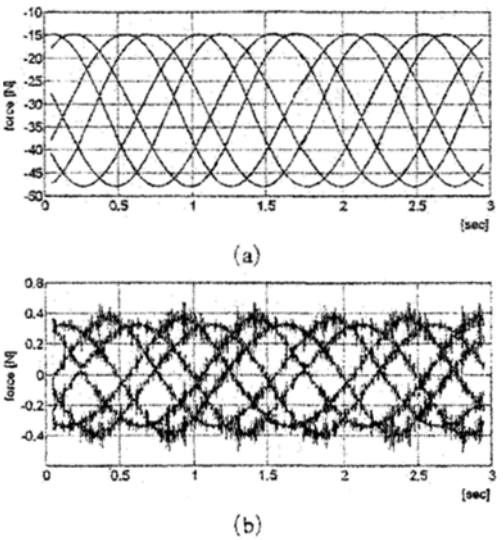

Fig. 7 (a) Actuator forces from DADS and MATLAB for a circle trajectory with 40 rpm speed, (b) Descrepancy between the actuator forces from DADS and MATLAB

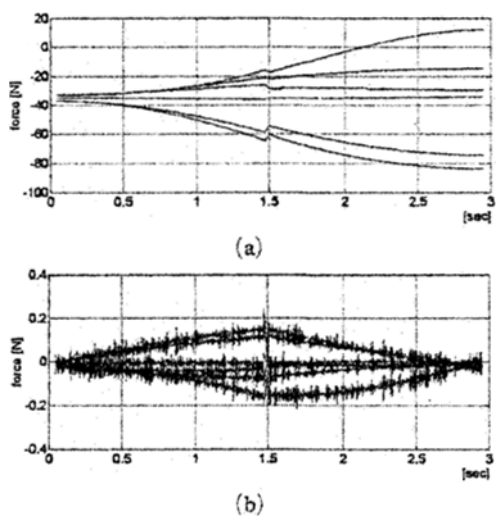

Fig. 8 (a) Actuator forces from DADS and MATLAB for a sample desired trajectory of the platform that is moving with a constant acceleration, (b) Descrepancy between the actuator forces from DADS and MATLA

4.2 Link inertia effect

The required actuator force due to link inertia

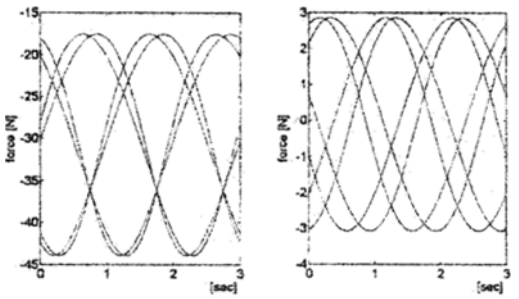

Fig. 9 Total actuator (a) and link inertia actuator force (b) (speed=20 rpm)

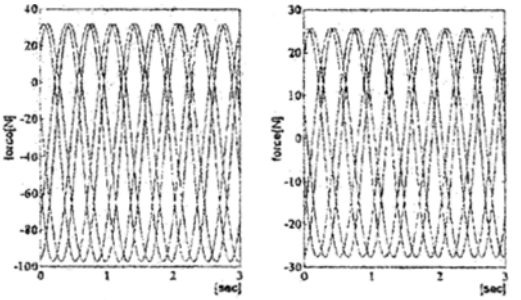

Fig. 10 Total actuator (a) and link inertia actuator force (b) (speed =60 rpm)

effect is derived from Eq. (29) as

$$\tau_{Li}=\frac{1}{l}\mathbf{a}_i^T\mathbf{n}_i^{\times}\mathbf{I}_{Li}\dot{\boldsymbol{\omega}}_{Li}+\frac{1}{l}\mathbf{a}_i^T\mathbf{n}_i^{\times}\boldsymbol{\omega}_{Li}^{\times}(\mathbf{I}_{Li}\boldsymbol{\omega}_{Li})+\frac{l}{4}m_{Li}\mathbf{a}_i^T(\mathbf{I}_{3\times3}+\mathbf{n}_i\mathbf{n}_i^T)\ddot{\mathbf{n}}_i+\frac{1}{2}m_{Li}\bar{\lambda}_i\mathbf{a}_i^T(\mathbf{I}_{3\times3}+\mathbf{n}_i\mathbf{n}_i^T)\mathbf{a}_i$$

$$-\mathbf{a}_i^T\mathbf{n}_i\gamma_i\mathbf{T}_1^{-1}\begin{bmatrix}\sum\left(\frac{1}{l}\mathbf{n}_i^{\times}\left(\mathbf{I}_{Li}+m_{Li}\left(\frac{l}{2}\right)^2\mathbf{I}_{3\times3}\right)\dot{\boldsymbol{\omega}}_{Li}+\frac{1}{l}\mathbf{n}_i^{\times}\boldsymbol{\omega}_{Li}^{\times}(\mathbf{I}_{Li}\boldsymbol{\omega}_{Li})+\frac{1}{2}m_{Li}\bar{\lambda}_i\mathbf{n}_i^{\times}\mathbf{n}_i^{\times}\mathbf{a}_i\right)\\ \sum GB_i^{\times}\left(\frac{1}{l}\mathbf{n}_i^{\times}\left(\mathbf{I}_{Li}+m_{Li}\left(\frac{l}{2}\right)^2\mathbf{I}_{3\times3}\right)\boldsymbol{\omega}_{Li}+\frac{1}{l}\mathbf{n}_i^{\times}\boldsymbol{\omega}_{Li}^{\times}(\mathbf{I}_{Li}\boldsymbol{\omega}_{Li})+\frac{1}{2}m_{Li}\bar{\lambda}_i\mathbf{n}_i^{\times}\mathbf{n}_i^{\times}\mathbf{a}_i\right)\end{bmatrix} \quad (34)$$

Note that a portion of the link inertia effect influences the actuator force directly, while the remaining portion influences the actuator force in a coupled way through the transpose of the Jacobian matrix. Since the actuators of HSM are fixed at the base, the link weight is smaller than that of Stewart platform in which the actuators are attached at the moving links. The link inertia effect in the HSM, therefore, may be insignificant given the the slow operation of the manipulator. Figure 9 shows the total actuator forces and actuator force generated only by the link inertia when the trajectory of the platform has the speed of 20 rpm for 100mm radius eircular motion. Figrue 10 shows the case when the speed is increased to 60 rpm. It is seen that the higher the speed, the more significant the link inertia effects. The link inertia, therefore, must be included in higher speed operations.

The calculation time of the inverse dynamic equations is an important factor in control applications. When the link inertia effects are included, it takes 16.59 sec in Pentium III 650 processor. When the link inertia effects are not included, it takes 8.52 sec. In each case, the simulation time is 3 sec with a 0.005 sec step size using the MATLAB program. Therefore, engineers can judge whether to include the link inertia term or not by the proposed dynamic equation simulation.

4.3 Joint friction effect

The actuator forces generated by the joint friction can be found from Eq. (32). The friction al force on the slider axis has direct influence on the actuator force. However, a portion of the frictional forces and moments of the universal or spherical joints have coupled effects through the Jacobian matrix. Therefore, the joint friction effects may be magnified depending on the characteristics of the Jacobian matrix. Figure 11 shows the actuator forces generated by a typical friction of the sliders, universal joints, and spherical joints when the trajectory of the platform has the speed of 20rpm for 100mm radius circular motion. As compared with the total actuator forces in Fig. 9(a), we can say that the frictions on the universal and spherical joints have small influence on the total actuator force for this particular simulation case. This is, however, caused by relatively small values of the frictional coefficients at the joints.

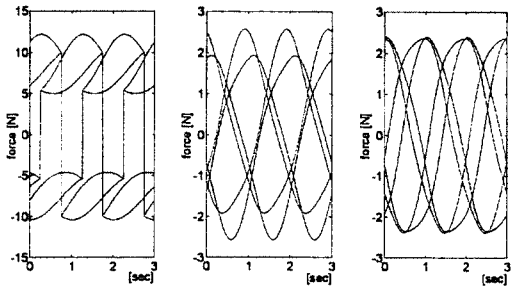

Fig. 11 Additional actuator forces due to frictions at (a) sliders, (b) universal joints, and (c) spherical joints

5. Conclusions

In this paper, inverse kinematic and dynamic analyses have been performed for PUS HexaSlide type parallel manipulators. The motion of the sliders, links, and platform is derived given the desired trajectory of the platform by applying the inverse kinematic analyses. The inverse dynamic equations of motion are derived by the Newton-Euler approach that uses the motion information of each body. In the derivation, the joint frictions as well as all the link inertia are included. Unlike the case of serial manipulators, the inverse dynamic equations involve coupled linear equations. Relative importance of the link inertia and joint frictions on the computed torque is investigated by computer simulations. It is expected that the inverse kinematic and dynamic equations can be used in the computed torque control and model-based adaptive control strategies.

Acknowledgement

This research was supported by the Brain Korea21 (BK21) fund from the Ministry of Education.

References

Codourey A., 1998, "Dynamic Modeling of Parallel Robots for Computed-Torque Control Implementation," *The International Journal of Robotic Research*, Vol. 17, No. 12, pp. 1325~1336.

Dasgupta B., and Mruthyunjaya T. S., 1998, "A Newton-Euler Formulation for the Inverse Dynamics of the Stewart Platform Manipulator," *J. Mech. Mach. Theory*, Vol. 33, No. 8, pp. 1135~1152.

Dasgupta B., and Choudhury P., 1999, "A General Strategy Based on the Newton-Euler Approach for the Dynamic Formulation of Parallel Manipulators," *J. Mech. Mach. Theory*. Vol. 34, pp. 801~824.

Gosselin C. M., 1996, "Parallel Computation Algorithms for the Kinematics and Dynamics of Parallel Manipulators," *J. of Dynamic Systems Measurement & Control-Transactions of the ASME*, V. 118 N. 1

Honegger M., 1998, "Nonlinear Adaptive Control of a 6 DOF Parallel Manipulator," *MOVIC '98, Zurich, Switzerland*, August 25-28, Vol. 3, pp. 961~966.

Ji A., 1993, "Study of the Effect of Leg Inertia in Stewart Platforms," *Proc. of the IEEE Conf. on Robot. and Automat. Los Alamitos, CA: IEEE*, pp. 121~126

Kim M. K., Park C. G., and Lee K. I., 1998, "Dynamic Analysis Considering the Effect of Leg Inertia and Design of Adaptive Controller in a Stewart Platform," *Proc. of '98 KSME fall annual meeting*, Vol. A., pp. 657~662.

Lebret G., Liu K., and Lewis F. L., 1993, "Dynamic Analysis and Control of a Stewart Platform Manipulator," *J. Robot. Sys.*, 10(5):629~655.

Lee C. W., and Kim N. N., 1999, "Model-Based Control System Design and Sliding Mode Control of Stewart Platform Manipulator," *Trans. of KSME*, A Vol. 23, No. 6, pp. 903~911.

Miller K., 1993, "The Proposal of a new Model of Direct-Drive Robot DELTA-4 Dynamics," *Proc. of '93 ICAR, the Int. Conf. on Robot.*, pp. 411~416.

Reboulet C., and Berthomieu T., 1991, "Dynamic Models of a Six-Degree-of-Freedom Parallel Manipulator," *Proc. of '91 ICAR, the Int. Conf. on Adv. Robot.*, vol. 2, pp. 1153~1157.

Toyoda, 1996, "Parallel Mechanism Based

Milling Machine," Cat. No. 96 1110-0 JO. Merlet, J-P., 1997, *Les Robots Paralleles*, 2^{e} éd., Hermès, Paris.

Appendix

A.1 Geometrical and dynamic parameters of a HSM

$$\mathbf{A}_{0,i}=\begin{pmatrix} -0.7380 & -0.8480 & -0.1100 & 0.1100 & 0.8480 & 0.7380 \\ -0.5531 & -0.3625 & 0.9157 & 0.9157 & -0.3625 & -0.5531 \\ 0.0000 & 0.0000 & 0.0000 & 0.0000 & 0.0000 & 0.0000 \end{pmatrix}$$

$$\mathbf{A}_{1,i}=\begin{pmatrix} -0.2130 & -0.3230 & -0.1100 & 0.1100 & 0.3230 & 0.2130 \\ -0.2500 & -0.0594 & 0.3095 & 0.3095 & -0.0594 & -0.2500 \\ 0.3500 & 0.3500 & 0.3500 & 0.3500 & 0.3500 & 0.3500 \end{pmatrix}$$

$$\mathbf{CB}'_i=\begin{pmatrix} -0.0515 & -0.1615 & -0.1100 & 0.1100 & 0.1615 & 0.0515 \\ -0.1567 & 0.0337 & 0.1229 & 0.1229 & 0.0337 & -0.1567 \\ 0.0000 & 0.0000 & 0.0000 & 0.0000 & 0.0000 & 0.0000 \end{pmatrix}$$

$c_{si}=0.001$, $\mu_{si}=0.2$, $\tau_b=0$

$c_{ui}=0.001$, $\tau_{ui}=0.006 \| \mathbf{F}_{Ai} \| \boldsymbol{\omega}_{li}/\| \boldsymbol{\omega}_{li} \|$

$c_{pi}=0.001$, $\tau_{pi}=0.006 \| \mathbf{F}_{Bi} \| (\boldsymbol{\omega}_{li}-\boldsymbol{\omega})/\| \boldsymbol{\omega}_{li}-\boldsymbol{\omega} \|$

$$\mathbf{I}'=\begin{pmatrix} 0.1181489 & 0 & 0 \\ 0 & 0.1181488 & 0 \\ 0 & 0 & 0.2258968 \end{pmatrix}$$

$$\mathbf{I}'_{li}=\begin{pmatrix} 0.1402837 & 0 & 0 \\ 0 & 0.1402837 & 0 \\ 0 & 0 & 0.0001087 \end{pmatrix}$$

$$\mathbf{g}=\begin{pmatrix} 0.00 \\ 0.00 \\ 9.81 \end{pmatrix}, \quad \mathbf{GC}'=\begin{pmatrix} 0.000 \\ 0.000 \\ -0.007 \end{pmatrix}$$

$l=0.9$m, $m=10.7673$kg, $m_{li}=2.1729$kg,

$m_{si}=0.9971$kg